

most susceptible to the impact of pollution aerosols on their albedo (27). However, the findings here suggest that this susceptibility does not translate into large sensitivity to anthropogenic land-based aerosols as currently believed, for two reasons: (i) Aerosols in a cloudy marine boundary layer are deposited quickly by cloud processes; and (ii) when pollution aerosols manage to interact with clouds over the sea, the sea salt reduces the supersaturation and hence the droplet concentrations and cloud albedo. These are likely causes for the larger cloud drop  $r_{\text{eff}}$  for the same aerosol index over the ocean as compared to land (28), recently observed by satellite, which has been unexplained until now.

## References and Notes

1. S. K. Satheesh, V. Ramanathan, *Nature* **405**, 60 (2000).
2. D. Rosenfeld, *Geophys. Res. Lett.* **26**, 3105 (1999).
3. D. Rosenfeld, *Science* **287**, 1793 (2000).
4. D. Rosenfeld, Y. Rudich, R. Lahav, *Proc. Natl. Acad. Sci. U.S.A.* **98**, 5975 (2001).
5. G. A. McFarquhar, A. Heymsfield, *J. Geophys. Res.* **106**, 28653 (2001).
6. D. Rosenfeld D., G. Gutman, *Atmos. Res.* **34**, 259 (1994).
7. A. P. Khain, D. Rosenfeld, A. Pokrovsky, *Geophys. Res. Lett.* **28**, 3887 (2001).
8. D. A. Hegg, Y. J. Kaufman, *J. Geophys. Res.* **103**, 5671 (1998).
9. D. Rosenfeld, I. M. Lensky, *Bull. Am. Meteorol. Soc.* **79**, 2457 (1998).
10. W. A. Cooper, R. T. Bruintjes, G. K. Mather, *J. Appl. Meteorol.* **36**, 1449 (1997).
11. C. D. O'Dowd, J. A. Lowe, M. H. Smith, A. D. Kaye, *Q. J. R. Meteorol. Soc.* **125**, 1295 (1999).
12. G. Feingold, W. R. Cotton, S. M. Kreidenweis, J. T. Davis, *J. Atmos. Sci.* **56**, 4100 (1999).
13. Y. Yin, Z. Levin, T. G. Reisin, S. Tzivion, *Atmos. Res.* **53**, 91 (2000).
14. Z. Levin, E. Ganor, V. Gladstein, *J. Appl. Meteorol.* **35**, 1511 (1996).
15. Y. Rudich, D. Rosenfeld, O. Khersonsky, *Nature*, in press.
16. M. A. LeMone, E. J. Zipser, *J. Atmos. Sci.* **37**, 2458 (1980).
17. C. Lucas, E. J. Zipser, M. A. LeMone, *J. Atmos. Sci.* **51**, 3183 (1994).
18. HYSPLIT4 is the Hybrid Single-Particle Lagrangian Integrated Trajectory model. Web address: <http://www.arl.noaa.gov/ready/hysplit4.html> (NOAA Air Resources Laboratory, Silver Spring, MD, 1997).
19. J. Lelieveld et al., *Science* **291**, 1031 (2001).
20. A. H. Woodcock, *J. Meteorol.* **10**, 362 (1953).
21. N. Sugimoto et al., *J. Mar. Meteorol. Soc. Jpn.*, **76**, 93 (2000).
22. B. A. Albrecht, *Science* **245**, 1227 (1989).
23. A. S. Ackerman, O. B. Toon, P. V. Hobbs, *Science* **262**, 226 (1993).
24. D. Rosenfeld, W. L. Woodley, *Meteorol. Monogr.*, in press.
25. D. Rosenfeld, C. W. Ulbrich, *Meteorol. Monogr.*, in press.
26. A. P. Khain, M. Ovtchinnikov, M. B. Pinsky, A. Pokrovsky, H. Krugliak, *Atmos. Res.* **55**, 159 (2000).
27. S. Twomey, *J. Atmos. Sci.* **34**, 1149 (1977).
28. F. M. Breon, D. Tanre, S. Generoso, *Science* **295**, 834 (2002).
29. The authors thank V. Ramanathan for provoking this study by asking "What happens to the air pollution over the Indian Ocean as it goes into the ITCZ?" This study was funded by the Israeli Space Agency and by the Israeli Water Commission. Funding was also provided by project EURAINSAT, a shared-cost project (contract EVG1-2000-00030) cofunded by the Research Directorate General of the European Commission within the research and technological development activities of a generic nature of the Environment and Sustainable Development subprogram (5th Framework Programme).

## Supporting Online Material

[www.sciencemag.org/cgi/content/full/1073869/DC1](http://www.sciencemag.org/cgi/content/full/1073869/DC1)  
Figs. S1 to S8  
References

13 May 2002; accepted 5 August 2002

Published online 15 August 2002;

10.1126/science.1073869

Include this information when citing this paper.

## REPORTS

## High Carrier Mobility in Single-Crystal Plasma-Deposited Diamond

Jan Isberg,<sup>1\*</sup> Johan Hammersberg,<sup>1</sup> Erik Johansson,<sup>1</sup>  
Tobias Wikström,<sup>1</sup> Daniel J. Twitchen,<sup>2</sup> Andrew J. Whitehead,<sup>2</sup>  
Steven E. Coe,<sup>2</sup> Geoffrey A. Scarsbrook<sup>2</sup>

Room-temperature drift mobilities of 4500 square centimeters per volt second for electrons and 3800 square centimeters per volt second for holes have been measured in high-purity single-crystal diamond grown using a chemical vapor deposition process. The low-field drift mobility values were determined by using the time-of-flight technique on thick, intrinsic, freestanding diamond plates and were verified by current-voltage measurements on *p-i* junction diodes. The improvement of the electronic properties of single-crystal diamond and the reproducibility of those properties are encouraging for research on, and development of, high-performance diamond electronics.

The desire for electronic devices with higher power throughput, wider frequency bandwidth, and higher operational temperatures is driving research and development of new semiconductors. One such area is wide-band-gap materials. Diamond is extreme in this group of materials,

which includes SiC, ZnO, and GaN, having a direct band gap of 7.5 eV, an indirect gap of 5.5 eV, and a room-temperature thermal conductivity in excess of 2000 W/mK. Diamond electronic devices, such as power diodes and high-frequency field-effect transistors, are expected to deliver outstanding performance because of the material's excellent intrinsic properties, such as high carrier mobilities and high breakdown field (1, 2). However, the development of diamond electronics has been hampered by several problems, such as a lack of shallow dopants, heteroepitaxy as a route to large-area single-crystal growth, low crystal quality, and poor

consistency of synthetic material. Nevertheless, interesting devices have been made; for example, Koizumi and co-workers have recently realized an ultraviolet light-emitting *p-n* diode in diamond (3).

Synthetic diamond has been produced for the past 50 years with high-pressure high-temperature (HPHT) technology and more recently by chemical vapor deposition (CVD). CVD offers a process for producing high-crystalline quality diamond under tightly controlled conditions. Although high-quality polycrystalline diamond with many properties that approach those of the best natural diamonds is now commercially available, the presence of grain boundaries impedes electronic performance, so that the only option for the most demanding applications is single-crystal CVD diamond. Despite more than 10 years of intensive research in this area, the best material suitable for electronic applications that has been reported is thin layers (typically  $\ll 100 \mu\text{m}$ ) having electronic properties, such as carrier mobility and lifetime, similar to those measured in specially selected natural type IIa diamond (4). Reported room-temperature values of carrier mobility ( $\mu$ ) in type IIa diamond are typically in the range of 2000 to 2800  $\text{cm}^2/\text{Vs}$  for electrons and 1800 to 2100  $\text{cm}^2/\text{Vs}$  for holes. This is the case for both Hall (5, 6) and drift (7, 8) mobility measurements. In homoepitaxial boron-doped CVD diamond, Yamanaka et al. (9) have measured a Hall hole mobility of 1840  $\text{cm}^2/\text{Vs}$ . Improvement in electronic properties such as carrier mobility and lifetime can be directly related to enhanced crystalline quality and reduced defect

<sup>1</sup>ABB Group Services Center, Corporate Research, Nanotechnology and Innovative Materials Group, Västerås, Sweden. <sup>2</sup>De Beers Industrial Diamonds, King's Ride Park, Ascot, UK.

\*Present address: Division for Electricity Research, Box 539, S-751 21 Uppsala University, Sweden. E-mail: jan.isberg@angstrom.uu.se

## REPORTS

(point and extended) concentration, because the carrier mobility is limited by defect-scattering mechanisms.

The samples discussed in this report were synthesized with a microwave plasma-assisted CVD reactor operating at a frequency of 2.45 GHz. For the time-of-flight (TOF) measurements, homoepitaxial CVD diamond layers were deposited on specially prepared  $\langle 100 \rangle$ -oriented HPHT synthetic diamond substrates measuring 4 by 4 by 0.5 mm. Care was taken to ensure that the surface quality of the substrates was as high as possible and that the substrates were free of metallic inclusions that can act as sources of dislocations in the epitaxial overlayer. A pre-growth etch phase was followed by epitaxial overgrowth under conditions of high purity. The growth conditions used were as follows: total gas flow of 700 standard cubic centimeters per minute (consisting of hydrogen with  $\sim 5.5\%$  methane and  $\sim 10\%$  argon), pressure of  $> 15$  kPa, and a substrate temperature ( $T$ ) of  $\sim 830^\circ\text{C}$ . After synthesis, the high-purity epitaxial overlayer was first separated from its HPHT diamond substrate by a laser cutting technique and then polished by means of standard lapidary techniques to give a freestanding high-purity plate. The plate thickness,  $L$ , ranged between 390 and 690  $\mu\text{m}$ . Finally, semitransparent titanium/aluminum/gold contacts, 4 mm in diameter, were formed on the  $\{100\}$  surfaces.

The  $p$ - $i$  junction diodes were grown using a technique similar to that used for the high-purity layers described above. Similar  $p$ - $i$  structures have previously been reported (10, 11). Heavily boron-doped layers were synthesized by addition of diborane ( $\text{B}_2\text{H}_6$ ) to the source gas mixture. The resulting concentration in the solid was  $1 \times 10^{20}$  boron atoms  $\text{cm}^{-3}$ , measured by secondary ion mass spectroscopy (SIMS). After removal from the HPHT substrate and subsequent polishing, thin high-purity layers were deposited on the boron substrates, producing  $p$ - $i$  structures with  $i$ -layer thicknesses ranging from 10 to 18  $\mu\text{m}$ . Ohmic contacts were fabricated on the boron-doped surface by implanting it with  $2 \times 10^{16}$   $\text{cm}^{-2}$  boron ions at 37 keV, followed by a high-vacuum anneal at  $1100^\circ\text{C}$ . Titanium/aluminum/gold contacts were then formed on this implanted surface by means of physical vapor deposition combined with standard lithography and wet chemical etching. The contacts were annealed in argon at  $600^\circ\text{C}$ . The finished  $p$ - $i$  junction diodes consisted of an ohmic contact to an  $\sim 300$ - $\mu\text{m}$ -thick boron-doped diamond layer supporting a thinner oxygen-terminated intrinsic layer with a blocking gold contact, 1 mm in diameter.

The intrinsic CVD diamond was characterized with Raman, electron paramagnetic resonance, SIMS, photoluminescence, cathodoluminescence (CL), X-ray rocking curve, transmission electron microscopy, and traditional absorption techniques. The material was found to be of exceptional purity with respect to in-

trinsic and extrinsic defects, showing a characteristically strong CL free-exiton signal at 235 nm and a measured total nitrogen concentration below  $1 \times 10^{15}$   $\text{cm}^{-3}$ . In addition, the growth conditions and careful substrate preparation resulted in a very low dislocation density ( $< 10^6$   $\text{cm}^{-2}$ ). It is to the low defect and dislocation densities that we attribute the high mobilities and long carrier lifetime reported below.

In the reverse direction, the best diodes were capable of blocking in excess of 2.5 kV, despite lacking any specifically designed edge termination. Figure 1 shows typical current-voltage ( $I$ - $V$ ) curves in the forward direction. The conductivity in the intrinsic layer of the diode is controlled by space charge-limited transport, which obeys the Mott-Gurney law  $j = 9/8 \epsilon \mu V^2/d^3$ , where  $j$  is the current density,  $\mu$  the hole drift mobility,  $V$  the bias, and  $d$  the thickness of the intrinsic layer. A series resistance was added to account for ohmic losses, and the hole injection is modeled assuming a simple Schottky model (12, 13). The hole mobility extracted from the fits is plotted in Fig. 2 for temperatures in the interval from 300 to 540 K. At 300 K, the hole mobility was measured to be  $4100 \pm 400$   $\text{cm}^2/\text{Vs}$ , which is a factor of 2 higher than is typically quoted for natural single-crystal diamond (14). For temperatures between 300 K <

$T < 380$  K, the mobility shows a  $T^{-3/2}$  dependence indicative of acoustic phonon scattering as the limiting mechanism; whereas at higher temperatures,  $400 \text{ K} < T < 540 \text{ K}$ , there exists a steeper dependence,  $\mu \sim T^{-3.7}$ , in agreement with previous results on high-purity, natural, type IIa diamond (15).

The TOF technique was used to determine the low-field drift mobilities of both electrons and holes. The samples were biased along the  $\langle 100 \rangle$  direction by means of a transmission line bias circuit with one surface illuminated through the semitransparent contact, using a quintupled 5-ns Nd:yttrium-aluminum-garnet (Nd:YAG) laser pulse with a repetition rate of 10 Hz. The quintupled Nd:YAG laser yields a strongly absorbed, above-bandgap, 213-nm laser pulse with only a 3- $\mu\text{m}$  penetration depth. The bias is applied in short pulses in order to minimize charge buildup and resulting polarization effects. The transient current was measured at a controlled temperature for various bias voltages. Parameters such as the carrier mobilities ( $\mu$  and  $\mu_n$ ) and carrier lifetime can be determined from the characteristic features in the transient current data. This method has previously been used to determine electron and hole-drift mobility in natural type IIa diamond (7, 8) in the low injection regime. Here we used TOF

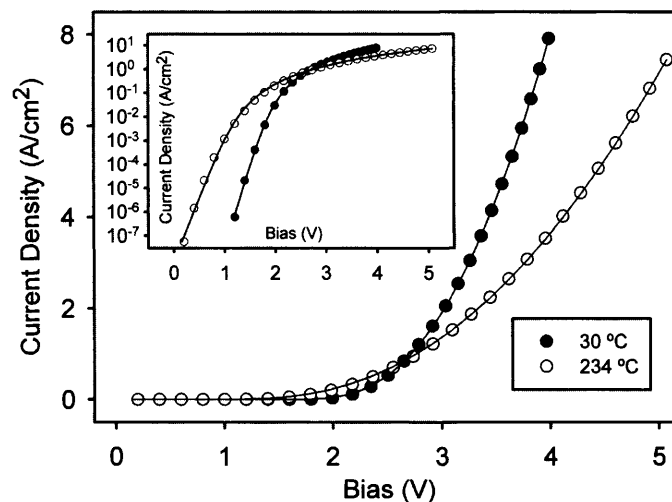


Fig. 1. Examples of measured forward  $I$ - $V$  data on the  $p$ - $i$  junction diodes, together with best fits from the model described in the text.

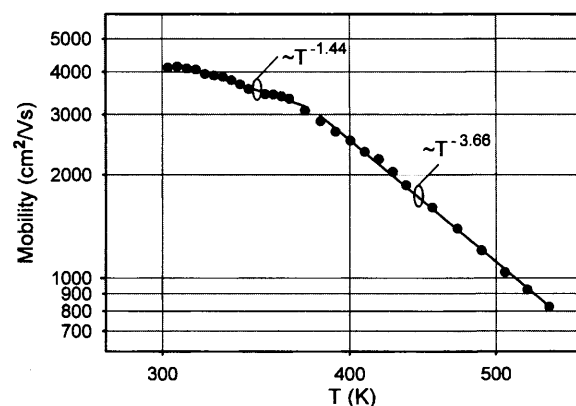


Fig. 2. Extracted mobility data from  $p$ - $i$  junction diode measurements versus temperature.

in the high injection regime, where the carrier transport is space charge-limited [for a theoretical background, see (16, 17)]. Near the illuminated electrode, a reservoir of carriers is created that is rapidly thermalized. The first current peak (Fig. 3) results from the screening of the field in this electron-hole plasma (18). Subsequently, carriers attracted by the bias move through the sample, and the second peak occurs at a time,  $\tau_{\text{TOF}}$ , when the first carriers reach the opposite electrode. The third broad current peak in Fig. 3 is attributed to ambipolar diffusion of the carrier plasma [referred to as the ambipolar diffusion and drift current (ADDC) peak in the following discussion]. The choice of bias polarity determines whether the transit of electrons or holes is observed. For low bias,  $\tau_{\text{TOF}}$  varies in inverse proportion to the bias  $U$  as  $\tau_{\text{TOF}} = \beta L^2 / \mu_{e,h} U$ , where  $\beta$  is a correction factor that depends on sample thickness and the light absorption profile (17). Deviations from unity are due to the inhomogeneous field distribution during the space charge-limited transit (SCLT).

To further understand the transient current data, the experiment was modeled by numerically solving the coupled drift-diffusion and Poisson's equations for various electron and hole mobility values. The simulated currents were found to be in excellent agreement with the experimental data. Using the calculated val-

ues of  $\beta$ , which varied between 0.66 and 0.71 depending on sample thickness, the low-field drift mobilities were extracted from the measured data. This method of combining the SCLT current technique with a numerical calculation of  $\beta$  was validated by measuring the carrier mobility in a sample of high-purity silicon, which showed excellent agreement with numbers reported in the literature (19, 20).

The TOF data for the CVD diamond samples, measured at 25°C, are plotted against  $U/\beta L^2$  (Fig. 4). From the data, it is clear that the room-temperature mobility can reach values as high as 4500 and 3800  $\text{cm}^2/\text{Vs}$  for electrons and holes, respectively. This value of the hole mobility is in agreement with the result obtained from the  $p$ - $i$  junction diodes. The distribution of the mobility values between the samples is related to variations in material quality (that is, the crystal perfection and defect density), but in every case the high values indicate the superior quality of the diamond over previously reported material.

For the SCLT and ADDC peaks to be observed in the experiments requires material of high quality in which the lifetimes of the electrons and holes are longer than the duration of the transport process responsible. The SCLT peak requires carrier lifetimes of several tens of nanoseconds, and the ADDC peak

requires carrier lifetimes in excess of a microsecond, corresponding to a charge collection distance at 1  $\text{V}/\mu\text{m}$  in excess of 10 cm. Only in the best quality single-crystal material can the ADDC peak be observed. By comparing with the simulations, it is possible to conclude that the carrier lifetime exceeds 2  $\mu\text{s}$  in these samples. This constitutes a dramatic improvement as compared with lifetimes previously observed in "high-quality" natural and polycrystalline CVD diamond samples (21).

The experimentally determined values for the electron and hole mobility of 4500 and 3800  $\text{cm}^2/\text{Vs}$ , respectively, as well as the long carrier lifetime, are indicative of a significant improvement in the electronic quality of thick, freestanding, single-crystal CVD diamond and represent a major step toward the realization of viable diamond electronic devices. Many problems concerning the fabrication of diamond devices remain to be solved, but these results and the performance of the  $p$ - $i$  diamond diode indicate that the potential of single-crystal CVD diamond as a wide-band-gap semiconductor is substantial and will eventually allow the expansion of the boundaries of electronics technology.

References and Notes

1. C. E. Weitzel, *Inst. Phys. Conf.* **142**, 765 (1996).
2. R. J. Trew, J.-B. Yan, P. M. Mock, *Proc. IEEE* **79**, 598 (1991).
3. S. Koizumi, K. Watanabe, M. Hasegawa, H. Kanda, *Science* **292**, 1899 (2001).
4. Type IIa diamond is the purest natural diamond, with low levels of nitrogen and boron impurities.
5. A. G. Redfield, *Phys. Rev.* **94**, 526 (1954).
6. P. Denham, E. C. Lightowers, P. J. Dean, *Phys. Rev.* **161**, 762 (1967).
7. F. Nava, C. Canali, C. Jacoboni, L. Reggiani, S. F. Kozlov, *Solid State Commun.* **33**, 475 (1980).
8. L. Reggiani, S. Bosi, C. Canali, F. Nava, S. F. Kozlov, *Phys. Rev. B* **23**, 3050 (1981).
9. S. Yamanaka, D. Takegushi, H. Wanatabe, H. Okushi, K. Kajimura, *Physica Status Solidi (a)* **174**, 59 (1999).
10. K. Miyata, K. Kobashi, D. L. Dreifus, *Diamond Relat. Mater.* **2**, 1107 (1993).
11. H. Shiomi, Y. Nishibayashi, N. Fujimori, *Jpn. J. Appl. Phys.* **29**, L2163 (1990).
12. D. P. Halliday, T. A. Coultier, J. W. Gray, P. N. Adams, in *Proceedings of the 24th International Conference on the Physics of Semiconductors* (World Scientific, Singapore, 1999), vol. 3, pp. F21-F26.
13. A. V. Denisenko, G. C. Kosaca, W. R. Farmer, in *Proceedings of the 25th Annual Conference of the IEEE Industrial Electronics Society* (IEEE, Piscataway, NJ, 1999), vol. 1, pp. 74-79.
14. L. S. Pan, D. R. Kania, Eds. *Diamond: Electronic Properties and Applications* (Kluwer Academic, Boston, 1995).
15. F. Nava et al., *IEEE Trans. Nucl. Sci.* **NS-26**, 308 (1979).
16. A. Many, G. Rakavy, *Phys. Rev.* **126**, 1980 (1962).
17. G. Juska, M. Viliunas, O. Klima, E. Sipek, J. Kocka, *Philos. Mag. B* **69**, 277 (1994).
18. V. G. Baru, Y. N. Temnitskii, *Sov. Phys. Semicond.* **5**, 1862 (1972).
19. G. Ottoaviani, L. Reggiani, C. Canali, F. Nava, A. Alberigi-Quaranta, *Phys. Rev. B* **12**, 3318 (1975).
20. C. Canali, C. Jacoboni, F. Nava, G. Ottaviani, A. Alberigi-Quaranta, *Phys. Rev. B* **12**, 2265 (1975).
21. J. Hammersberg et al., *Diamond Relat. Mater.* **10**, 574 (2001).

Fig. 3. Experimental TOF for a 690- $\mu\text{m}$ -thick single-crystal CVD diamond sample with a bias of 30 V (with cathode illuminated) at 25°C. The characteristic features of the curve are explained in the text.

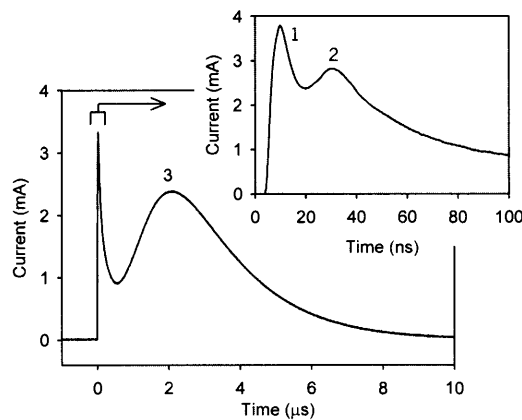
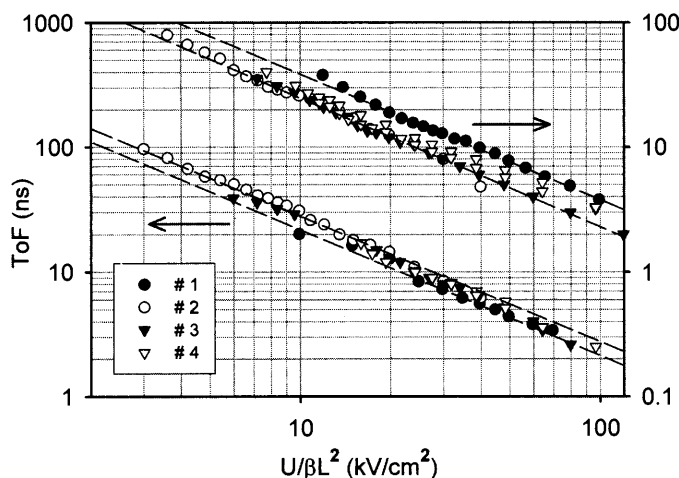


Fig. 4. TOF data (symbols) measured at 25°C for electrons (left scale) and holes (right scale). The dashed lines indicate the minimum and maximum mobilities measured: 3500 to 4500  $\text{cm}^2/\text{Vs}$  for electrons and 2600 to 3800  $\text{cm}^2/\text{Vs}$  for holes. Sample thickness and correction factors are as follows: #1,  $L = 391 \mu\text{m}$ ,  $\beta = 0.66$ ; #2,  $L = 690 \mu\text{m}$ ,  $\beta = 0.71$ ; #3,  $L = 496 \mu\text{m}$ ,  $\beta = 0.68$ ; #4,  $L = 391 \mu\text{m}$ ,  $\beta = 0.69$ .



28 May 2002; accepted 26 July 2002